First-principles determination of the tensile and slip energy barriers for $B2$ NiAl and FeAl

Ruqian Wu
Department of Physics and Astronomy, California State University, Northridge, California 91330-8268

Lieping Zhong
Department of Physics and Astronomy, Northwestern University, Evanston, Illinois 60208-3112

Lu-jun Chen
Department of Physics and Astronomy, California State University, Northridge, California 91330-8268

A. J. Freeman
Department of Physics and Astronomy, Northwestern University, Evanston, Illinois 60208-3112

(Received 8 April 1996)

The Griffith energies and the unstable stacking fault energies for FeAl and NiAl are investigated using the highly precise full potential linearized augmented plane wave method. Large multilayer relaxation is obtained through atomic force and total-energy calculations. The unstable stacking fault energies for $\langle 100\rangle$ and $\langle 110\rangle$ slips in NiAl(001) are 1.3 and 2.2 J/m^2, respectively. They are much smaller than the tensile cleavage energy, 5.4 J/m^2, and indicate that the major deformation mode in stoichiometric NiAl is $\langle 100\rangle$ slip, a result which agrees with experiment. For FeAl(001), the unstable stacking fault energies are much higher and are equally anisotropic (2.4 and 3.9 J/m^2 for $\langle 100\rangle$ and $\langle 110\rangle$ slips, respectively). We found that p-d hybridization plays an important role at E_F for NiAl but not for FeAl, which may contribute to these different mechanical properties. [S0163-1829(96)08034-4]

I. INTRODUCTION

B2 transition aluminides, especially FeAl and NiAl, have been extensively studied as high-temperature structural materials due to their intriguing properties such as high melting point, low specific gravity, good thermal conductivity, and oxidation resistance.[1–4] The long-range order produces strong bonding between atoms, which, in turn, usually leads to slower diffusion processes and better creep resistance.[5] To apply these materials to the aerospace industry, however, one must first overcome their disadvantages, i.e., the apparent poor ductility and low fracture toughness at ambient temperatures. Due to the intrinsic complexities of the mechanical processes, the mechanisms governing the ductile and brittle properties of intermetallic materials are still far from being well understood, and so challenge theoretical explanation.[6,7,11,8]

It is widely believed that the ductility of a material is closely related to the anisotropy of the energy surface encountered in the tensile and slip deformations.[9,10] When tensile stress applied at the tip of the crack exceeds the bond strength, the bonds there become unstable and the crack will extend, which results in brittle behavior. On the other hand, if the stress can be released through slip deformations, the crack is expected to be blunt and thus ductile behavior develops.[9] The resistance to the dislocation emission at a crack tip is associated to the energy barrier to slip deformation. The intrinsic ductile and brittle behavior is believed to be determined by a combination of three important quantities, namely, the Griffith energy (γ_s), the unstable stacking fault energy ($\gamma_{\rm us}$), and the product of shear modulus and Burgers vector. The ratio of $\gamma_s/\gamma_{\rm us}$ was proposed as a criterion for the intrinsic ductile and brittle properties for the case with a single sharp crack in a dislocation-free crystal.[10] However, it was found very recently that the ductile-brittle crossover is determined by a critical value of $\gamma_{\rm us}$, with increasing $\gamma_{\rm us}$ leading to reduced ductility.[11] The number of possible slip planes[12] and the anisotropy of the γ surface for a generalized stacking fault[13] are also believed to be important.

Unfortunately, only tensile energies for FeAl and NiAl have been determined using first-principles approaches based on the local-density-functional scheme.[6,11,8] Due to the inevitable large atomic relaxations and reconstructions, it is very difficult to obtain reliable results for the energy barriers for slip deformations and the full γ surface.[14] The values of $\gamma_{\rm us}$ are thus usually estimated indirectly from the energies for the antiphase boundaries, for which the effects of relaxation and reconstruction are assumed to be small. However, it was realized very recently that even a small relaxation can be very essential in the formation of the intermetallic compounds. For example, a correct structure (DO_{23}) for Al_3Ti can be obtained only when structural relaxations are considered.[15]

Here we directly determine the tensile cleavage (Griffith) energy γ_s, and the slip energy barriers $\gamma_{\rm us}$ (for $\langle 100\rangle$ and $\langle 110\rangle$ deformations) for the (001) plane of FeAl and NiAl using the full potential linearized augmented plane wave (FLAPW) method.[16] With the aid of total energy and atomic force approaches,[17] we optimize the positions of all the atoms in the unit cell. After a brief description of the methodology in Sec. II, calculated results of atomic structures, total energies, and the bonding mechanism are given in Secs. III and IV, respectively. Finally, a discussion and conclusion are presented in Sec. V.

TABLE I. The calculated interlayer distances (in a.u., where layer 1 is the surface layer) for the clean and slipped FeAl(001) and NiAl(001) surfaces and the energy barriers (in J/m^2) obtained from a seven-layer slab. Elements in parentheses denote those on the topmost layer.

System	d_{34}	d_{23}	d_{12}	γ_{us}
		clean		
FeAl (Al)	2.70	2.81	2.34	
FeAl (Fe)	2.63	2.62	2.53	
NiAl (Al)	2.65	2.73	2.55	
NiAl (Ni)	2.62	2.80	2.29	
		$\langle 100 \rangle$ slipped		
FeAl (Al)	2.70	3.81	2.22	2.29
FeAl (Fe)	2.62	3.63	2.43	2.54
NiAl (Al)	2.76	3.73	2.17	1.24
NiAl (Ni)	2.39	3.60	2.22	1.36
		$\langle 110 \rangle$ slipped		
FeAl (Al)	2.63	4.47	2.19	3.75
FeAl (Fe)	2.43	4.41	2.48	4.11
NiAl (Al)	2.82	4.52	2.12	2.14
NiAl (Ni)	2.34	4.34	2.29	2.34

II. METHODOLOGY AND COMPUTATIONAL DETAILS

In the FLAPW method,[16] no shape approximations are made for charge density, potential, and wave functions. The core states are treated fully relativistically, and the valence states are treated semirelativistically (i.e., without spin-orbit coupling). We employ the Hedin-Lundqvist formulas for the exchange-correlation potentials. This approach has been applied very successfully in the last decade to determine the electronic and magnetic properties of many transition-metal systems.[18]

Energy cutoffs of 13 and 100 Ry are employed for variational plane-wave bases and star functions to describe the wave functions and the charge density and potential in the interstitial region, respectively. Within the muffin-tin (MT) spheres ($r_{MT,Fe}=2.2$ a.u., $r_{MT,Ni}=2.0$ a.u., and $r_{MT,Al}=2.0$ a.u.), lattice harmonics with angular momentum l up to 8 are adopted. Convergence is assumed when the average root-mean-square difference between the input and output charge densities is less than 2×10^{-4} e/(a.u.)^3. The equilibrium geometries are determined with a criterion that the force on each atom is less than 2 m Ry/a.u.

III. ATOMIC STRUCTURE AND TOTAL ENERGY

A. Multilayer relaxation on NiAl(001) and FeAl(001)

The (001) surfaces of NiAl and FeAl have a simple structure and are ideally composed of either Ni(Fe) or Al atoms depending on where the lattice is truncated. In the present calculations, possible surface interdiffusion is excluded.[1] We used a seven-layer slab to simulate the NiAl(001) and FeAl(001) surfaces with either Al or Ni(Fe) as the topmost layer. The calculated equilibrium lattice constant of the $B2$ bulk NiAl and FeAl, namely, 5.36 and 5.31 a.u., are used in the lateral plane. The vertical positions of all atoms are optimized through their atomic forces.

As listed in Table I, the optimized interlayer distances indicate that the thickness of the slab is reasonably sufficient since the the calculated values of d_{34} are close to the distances between the adjacent Ni(Fe)-Al planes in the bulk, 2.68 a.u. (2.65 a.u.). Large surface relaxations are found for all cases. For the Al-truncated FeAl(001) and NiAl(001) surfaces, a large contraction (5–15 %) in d_{12} is accompanied by an expansion (2–6 %) in d_{23}. The calculated d_{12}, d_{23}, and d_{34} values for Al-truncated FeAl(001) are 2.34, 2.81, and 2.70 a.u. They are in excellent agreement with the measured results, i.e., 2.34 ± 0.04, 2.82 ± 0.04, and 2.77 ± 0.04 a.u., respectively.[19]

For NiAl(001), the surface relaxations reduce the surface energy by 109 meV for the Ni truncated case, and by only 18 meV for the Al truncated case. As a result, the cleavage energy of NiAl along the (001) direction is 5.4 J/m^2, a result which is very close to that obtained by Yoo and Fu for the unrelaxed case, 5.5 J/m^2.[20] Interestingly, we found that the value of the tensile cleavage energy is not sensitive to the approach adopted: Very close results (within 5%) are obtained through either (i) the asymptotic total-energy difference obtained as a function of the separation between two pieces stretched directly, or (ii) from the sum of surface energies of the Al and Ni truncated surfaces. For FeAl(001), the effects of surface relaxation are found to be stronger on the surface energies; the calculated tensile cleavage energy for FeAl along the (001) direction is 6.5 or 0.3 J/m^2 smaller than the unrelaxed value.[21]

B. Energy barriers for slip deformations

The predominance of $\langle 100 \rangle$ slip in NiAl ($\langle 111 \rangle$ in FeAl) has been well established.[22,23] However, due to difficulties in handling the inevitable large structural relaxation and reconstruction, first-principles calculations have rarely been done for the unstable stacking fault energy. For several systems such as Ni_3Al, Ni and Fe, γ_{us} was estimated using the embedded-atom method for investigating the mechanism of the brittleness of Ni_3Al.[24]

Here, two models are adopted for the determination of γ_{us}: (i) a four-layer slab model, in which the two upper layers are translated against the two bottom layers; (ii) a

seven layer slab model, in which the central three layers are translated against the outermost two layers on each side. The vertical positions of all the atoms are adjusted according to their atomic forces after the lateral translations. As a result, we found that the two models give close results (the difference is less than 0.2 J/m^2 for NiAl).

The optimized interlayer distances for the seven-layer slip deformed NiAl(001) and FeAl(001) slabs are listed in Table I. Surprisingly, the interlayer distance d_{34} is not compressed much for both $\langle 100 \rangle$ and $\langle 110 \rangle$ slips. In fact, it even expands in some cases compared to the values of d_{34} for clean NiAl(001) and FeAl(001) surfaces. On the other hand, the changes in d_{12} due to slip deformation are also less than 7% [except for NiAl(001), with Al as the topmost layer]. Thus the surface and interface effects in FeAl and NiAl are mostly localized within one and two layers.

The calculated energy barriers are listed in Table I. For NiAl, we found that the energy barriers for $\langle 100 \rangle$ and $\langle 110 \rangle$ slips are 1.30 and 2.20 J/m^2, respectively. Clearly, the γ surface for NiAl is strongly anisotropic, and the $\langle 100 \rangle$ Burger's vector appears to be the major slip direction for NiAl—a result which agrees with experiment.[1] A strong anisotropy is also found for the potential barrier of FeAl(001). For both $\langle 100 \rangle$ and $\langle 110 \rangle$ slips, the potential barriers for FeAl are about 70% higher than those for NiAl.

It is important to note that the multilayer relaxation is very important for the determination of the energy barriers. The calculated energy barrier for a rigid (without atomic relaxation) $\langle 100 \rangle$ slip in Ni(001) is 3.52 J/m^2, which is about three times larger than the value for the relaxed case. In addition, the slip-induced multilayer relaxation appears to be very sensitive to the surface truncation. The values of γ_{us} also depend on the trucation since, as listed in Table I, the calculated γ_{us} for Al-truncated cases are about 10% smaller than those for the Fe(Ni)-truncated cases. Together with the results obtained from the four-layer slabs, the error bar (because of the use of different models) for the determination of γ_{us} should be within 10%.

IV. BONDING MECHANISM

A. Bulk NiAl and FeAl

Obviously, accurately determined electronic properties are essential for understanding the mechanical behavior of materials. From the bonding charge densities (which are obtained by subtracting the superimposed atomic charge density from the self-consistent charge density) for bulk FeAl and NiAl given in Fig. 1, it is obvious that charge transfer

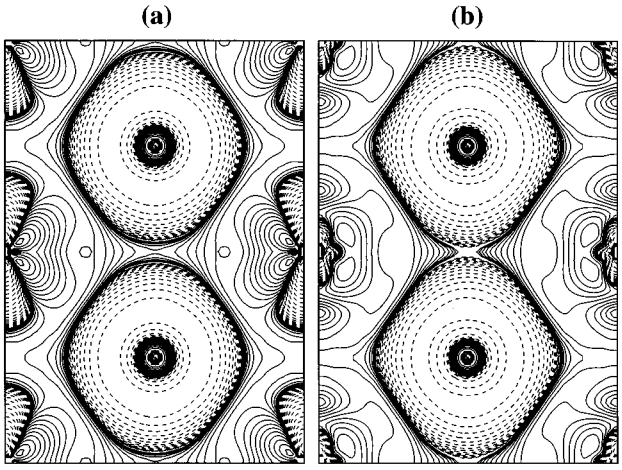

FIG. 1. The calculated bonding charge densities for (a) FeAl and (b) NiAl obtained by subtracting the superimposed Fe(Ni) and Al atomic charges from the corresponding self-consistent charge density. Contours start from $\pm 1 \times 10^{-4}$ e/a.u.^{3}, and increase successively by a factor of $\sqrt{2}$.

from Al to the transition-metal sites plays a dominant role. The Al thus acts as an electropositive element, and the repulsion between Al atoms is crucial for the structural ordering of these alloys.[1,20] In fact, this is also the driving force for the large multilayer surface rippling on the NiAl(110) surface.[25]

It is important to note here that the sign of the charge transfer obtained agrees with a simple estimate made from the Pauli electronegativities of Al (1.61), Ni (1.91), and Fe (1.83). An oppositely signed charge transfer was previously proposed by Liu *et al.*[26] based on the calculated [using the linearized-augmented Slater-type-orbital (LASTO) method] and the measured change of core-level binding energies for Ni and Al. To clarify this difference, we also calculated the core-level binding energies for bulk NiAl, Ni, and Al. Interestingly, as listed in Table II, the Ni (Al) core-level binding energies enhance (decrease) while charge accumulates (depletes) in the surrounding area. This unique behavior indicates the complexity of aluminides, and thus all aspects are needed to be considered for interpreting results.

Comparing the bonding charge density of FeAl and NiAl in Fig. 1, we found that the charge depletion from the Al sites is stronger in NiAl; the Al muffin-tin sphere in NiAl has 0.08 fewer electrons than that in FeAl. In addition, the bonding charge around Fe sites in Fig. 1(a) appears to be more directional than that around Ni in Fig. 1(b). More details

TABLE II. The calculated and measured core-level binding energies (in eV) for bulk NiAl, Ni, and Al.

Core	NiAl	Bulk Ni (Al)	ΔE_B FLAPW	ΔE_B LASTO [a]	Expt. [a]
Ni $3p_{3/2}$	62.96	62.44	0.52	0.26	0.4
Ni $2p_{3/2}$	830.46	830.19	0.27	0.2	0.4
Ni $2p_{1/2}$	847.90	847.64	0.26	0.2	0.2
Al $2p_{3/2}$	64.11	64.69	−0.58	−0.5	−0.2
Al $2s$	102.06	102.63	−0.57	−0.5	−0.3

[a]Reference 26.

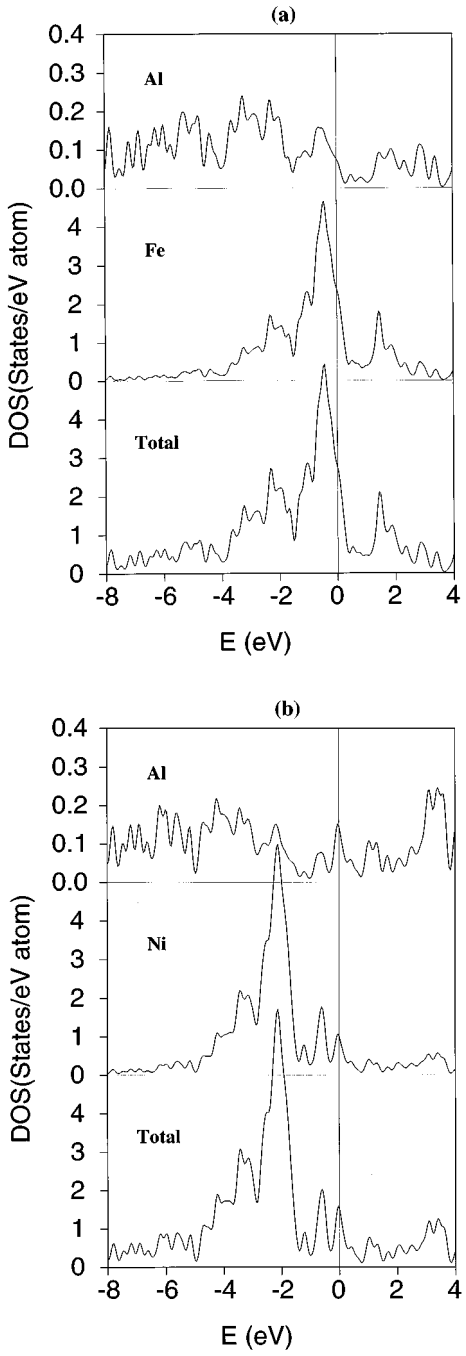

FIG. 2. The calculated density of states for (a) FeAl and (b) NiAl.

about the electronic interaction can be seen from the total and muffin-tin-projected density of states in Fig. 2. Clearly, no strong Al s,p–Ni(Fe) d resonant features are found for both systems (most of the resonant peaks in Al appear to originate from the tail effects). However, there is a pronounced peak at E_F for NiAl. As indicated in Fig. 3(b) by the energy-sliced charge density (from states within ± 0.2 eV), we can see that this peak originates from the hybridization between the Al p and Ni d_{z^2} states (both atoms contribute to the charge density). By contrast, Fe $d_{xz,yz}$ states dominate the charge distribution in Fig. 3(a) except for the very near nuclear region around the Al sites. This may be an important factor for the difference between the ductilities of

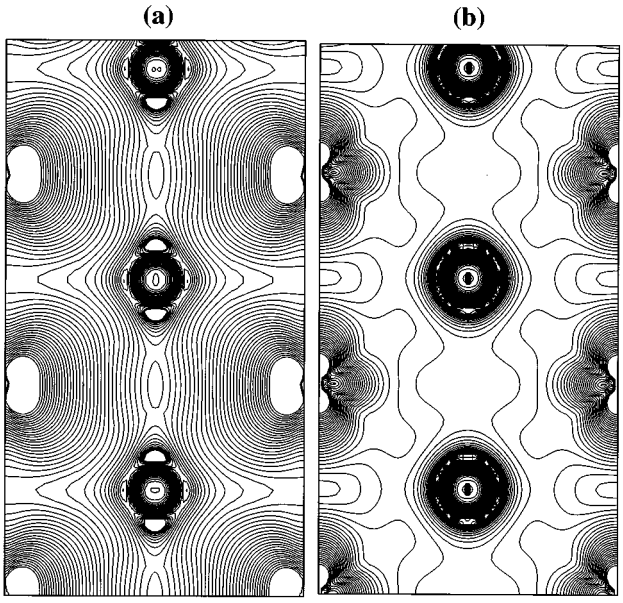

FIG. 3. The calculated charge densities at E_F for (a) FeAl and (b) NiAl. Contours start from $\pm 1\times 10^{-4}$ e/a.u.^{3}, and increase successively by a factor of $2^{1/4}$.

FeAl and NiAl. For a small distortion, which only affects states around E_F, Al $3p$ states are important in NiAl but not in FeAl.

B. Clean and slipped FeAl(001) and NiAl(001)

The bonding charge density of the FeAl(001) and NiAl(001) surfaces is plotted in Fig. 4 for the case with Al as the topmost layer. Clearly, the Al atoms also act as charge donors in the surface environment. Contours in the interior region resemble the bulk character for each system. In fact,

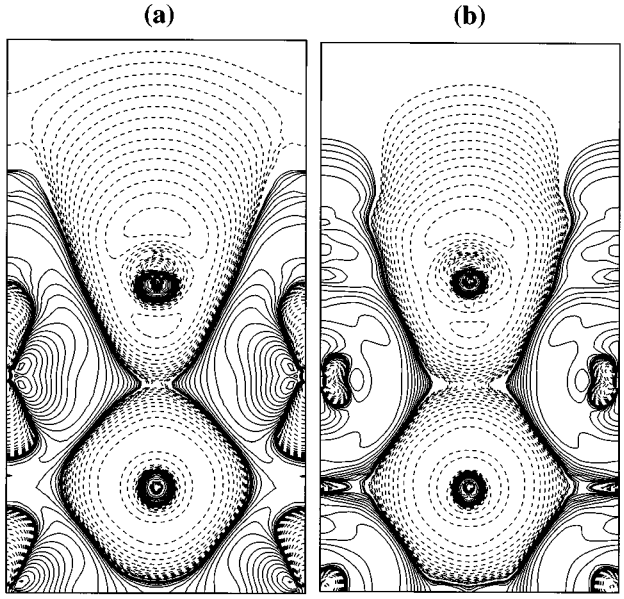

FIG. 4. The calculated bonding charge densities for (a) FeAl(001) and (b) NiAl(001). Contours start from $\pm 1\times 10^{-4}$ e/a.u.^{3}, and increase successively by a factor of $\sqrt{2}$.

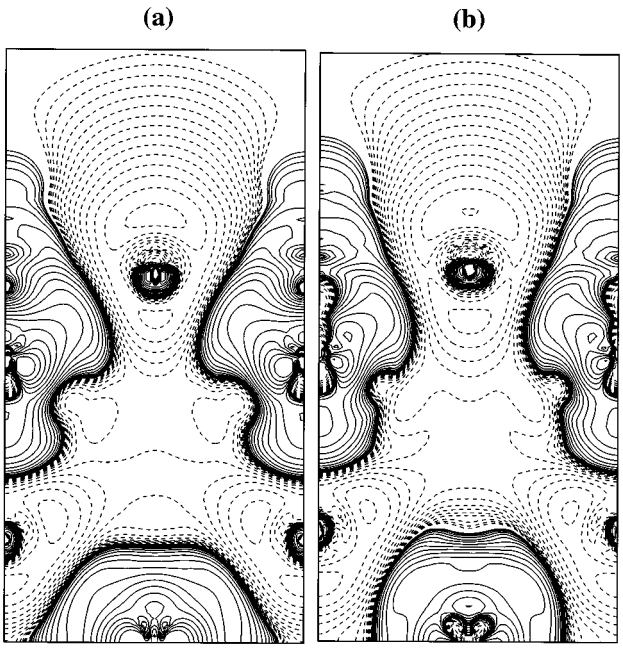

FIG. 5. The calculated bonding charge densities for $\langle 110\rangle$-slipped (a) FeAl(001) and (b) NiAl(001). Contours start from $\pm 1\times 10^{-4}$ e/a.u.^{3}, and increase successively by a factor of $\sqrt{2}$.

the numbers of electrons in the interior Al and Fe (Ni) muffin-tin spheres are very close to the corresponding bulk values (deviations of ± 0.03 electrons are due to relaxation). This strong screening effect ensures the validity of the calculated slip deformation energies with the present slab model.

For the deformed geometries, the bonding charges also show very similar behavior. The charge redistribution of $\langle 110\rangle(001)$ slipped FeAl and NiAl in Fig. 5, for instance, indicates that electrons deplete from the Al sites and accumulate at transition metal sites. However, the contours in the interfacial region show stronger spatial anisotropy—suggesting enhanced hybridization. Note that the Fe(Ni) bond lengths in the deformed NiAl and FeAl systems are only about 2–4 % shorter than that in their clear surface geometries. Thus a constant bond length appears to be a good approximation if one wants a quick approximate estimate of the γ surface.

V. DISCUSSION AND CONCLUSION

Although the results for the $\langle 111\rangle$ slips are not available now (calculations are in progress), we can attempt to find some clue from the available data for the key factors determining the ductile and brittle properties of an intermetallic material. Since FeAl (ductile) and NiAl (brittle, but fracture occurs after a substantial plastic deformation[27]) appear opposite in properties, it is interesting to compare possible factors.

First, is the anisotropy of the γ surface of crucial importance? This appears unlikely based only on the energy barriers for the $\langle 100\rangle$ and $\langle 110\rangle$ slips. As listed in Table I, $\gamma_{us,\langle 100\rangle}/\gamma_{us,\langle 110\rangle}$ for NiAl is 0.58, which is only slightly larger than that for FeAl, 0.61. Of course, since the major slip mode in FeAl is $\langle 111\rangle$ whereas it is $\langle 100\rangle$ in NiAl, results for $\langle 111\rangle$ slip are needed for any conclusion to be drawn.

Second, is the ductile/brittle property determined by the ratio of γ_s/γ_{us} (known as the Rice criterion)?[10] The value of γ_s/γ_{us} for NiAl is 4.2, which is even larger than that for FeAl, 2.7 (here $\langle 100\rangle$ slip barriers are used for both cases). Unless the energy barrier for the $\langle 111\rangle$ slip in FeAl is much lower than that for the $\langle 100\rangle$ slip (by a factor of at least 1.5), the Rice criterion appears not to be applicable for FeAl and NiAl.

Other possible reasons for the difference in mechanical properties between NiAl and FeAl include (i) the number of slip channels (four for FeAl and three for NiAl), and (ii) subtle differences for states at E_F. [For (ii) it is most probable that the directional p-d hybridization at E_F may contribute to reducing the ductility of NiAl, since it does not occur in FeAl.]

ACKNOWLEDGMENT

This work was supported by the Air Force Office of Scientific Research (Grant No. F49620-95-1-0189). We thank Y. Gornostyrev and O. Mryasov for helpful discussions.

[1] R.D. Noebe, R.R. Bowman, and M.V. Nathal, Int. Mater. Rev. **38**, 193 (1993).
[2] I. Baker and P.R. Munroe, in *High Temperature Aluminides and Intermetallics*, edited by S.H. Whang, C.T. Liu, and D. Pope (Metallurgical Society of AIME, Warrendale, PA, 1989), p. 425.
[3] M.H. Yoo, T. Takasugi, H. Hanada, and O. Izumi, Mater. Trans. JIM **31**, 435 (1990).
[4] R.L. Fleischer, D.M. Dimiduk, and H.A. Lipsitt, Ann. Rev. Mater. Sci. **19**, 231 (1989).
[5] M.H. Yoo, S.L. Sass, C.L. Fu, M.J. Mills, D.M. Dimiduk, and E.P George, Acta Metall. Mater. **41**, 987 (1993).
[6] T. Hong and A.J. Freeman, Phys. Rev. B **43**, 6446 (1991); J. Mater. Res. **7**, 68 (1992).
[7] J. Zou and C.L. Fu, Phys. Rev. B **51**, 2115 (1995).
[8] C.L. Fu and M.H. Yoo, Acta Metall. **40**, 703 (1992).
[9] J.R. Rice and R.M. Thomson, Philos. Mag. **29**, 73 (1973).
[10] J.R. Rice, J. Mech. Phys. Solids. **40**, 239 (1992).
[11] S.J. Zhou, A.E. Carlsson, and R. Thomson, Phys. Rev. Lett. **72**, 852 (1994).
[12] R. von Mises and Z. Angew, Math. Mech. **8**, 1599 (1963).
[13] V. Vitek, Cryst. Lattice Defects **5**, 1 (1974).
[14] Very recently, the γ surfaces for $B2$ FeAl and NiAl were calculated using the full potential linearized muffin-tin orbital method. A rigid shift mode (no relaxation) was adopted for analysis of ductile and brittle properties based on the Peierls-Nabarro model. For details, see N.I. Medvedeva, O.N. Mryasov, Y.N. Gornostyrev, D.L. Novikov, and A.J. Freeman (unpublished).
[15] C. Amador, J.J. Hoyt, B.C. Chakoumakos, and D. de Fontaine, Phys. Rev. Lett. **74**, 4955 (1995).

[16] E. Wimmer, H. Krakauer, M. Weinert, and A.J. Freeman, Phys. Rev. B **24**, 864 (1981); M. Weinert, E. Wimmer, and A.J. Freeman, *ibid.* **26**, 4571 (1982).

[17] J.M. Soler and A.R. Williams, Phys. Rev. B **40**, 1560 (1989); R. Yu, D. Singh, and H. Krakauer, *ibid.* **43**, 6411 (1991); R.Q. Wu and A.J. Freeman (unpublished).

[18] A.J. Freeman and R.Q. Wu, J. Magn. Magn. Mater. **100**, 497 (1991).

[19] H. Graupner, M. Kottcke, K. Heinz, and D.M. Zehner (unpublished).

[20] C.L. Fu and M.H. Yoo, in *High Temperature Ordered Intermetallic Alloys IV*, edited by L. Johnson, O. P. Pope, and J. D. Stiegler, MRS Symposium Proceedings No. 213 (Materials Research Society, Pittsburgh, 1991), p. 667; Mater. Sci. Eng. A **153**, 470 (1992).

[21] Using an unsaturated stretch (6.0 a.u.), Yoo and Fu obtained a smaller value of γ_s for the unrelaxed FeAl(001) lattice, 6.5 J/m^2 [see M.H. Yoo and C.L. Fu, ISIJ Int. **31**, 1049 (1991)].

[22] See, for example, A. Ball and R.E. Smallman, Acta Metall. **14**, 1517 (1966).

[23] T. Yamagata and H. Yoshida, Mater. Sci. Eng. **12**, 95 (1973).

[24] Y. Sun, J.R. Rice, and L. Truskinovsky, in *High Temperature Ordered Intermetallic Alloys IV* (Ref. 20), p. 243; J.R. Rice, G.E. Beltz, and Y. Sun, in *Topics in Fracture and Fatigue*, edited by A.S. Argon (Springer-Verlag, Berlin 1992).

[25] J.I. Lee, C.L. Fu, and A.J. Freeman, Phys. Rev. B **36**, 9318 (1987).

[26] S.C. Liu, J.W. Davenport, E.W. Plummer, D.M. Zehner, and G.W. Fernando, Phys. Rev. B **42**, 1582 (1990).

[27] V.I. Levit, I.A. Bul, J. Hu and M.J. Kaufman, Scr. Metall. (to be published).